Optimal Excitation Transfer in two-dimensional Lattices of Rydberg Atoms

Bachelorarbeit im Fach Physik
eingereicht von
Dominik Bäuerle

Fakultät für Mathematik und Physik
Albert-Ludwigs-Universität Freiburg
03.08.2017

Zusammenfassung Die vorliegende Arbeit widmet sich der Untersuchung von optimalem Transport einer einzelnen Anregung in Netzwerken von vier bis acht Rydberg-Atomen mittels Dipol-Dipol-Wechselwirkung. Die Anregung soll hierbei zwischen zwei festgelegten Atomen, die als Eingang und Ausgang bezeichnet werden, mit möglichst hoher Effizienz in möglichst kurzer Zeit übertragen werden. Durch experimentell realisierbare Bedingungen motiviert legen wir zunächst besonderes Augenmerk auf Netzwerke, deren einzelne Atome sich auf Punkten eines zweidimensionalen Gitters befinden. Wir beginnen mit einer Analyse aller Konfigurationsmöglichkeiten einer gewählten Gitterform, welche durch einfaches Ausprobieren zugänglich sind. Da wir für diesen Fall keine Übertragungseffizienzen von exakt 100% finden, betrachten wir als nächstes den allgemeineren Fall, in welchem die Atome auf beliebige Positionen im zweidimensionalen Raum (d.h. ohne Beschränkung auf bestimmte Gitterpunkte) platziert werden können. Hier finden wir eine diskrete, endliche Menge an „perfekten" Konfigurationen, d.h. solche, welche Effizienzen von 100% innerhalb kurzer Zeit ermöglichen.

Es stellt sich dadurch die Frage, warum unsere numerische Optimierung zwar eine diskrete Menge einzelner perfekter Konfigurationen, jedoch keine kontinuierlichen, parametrisierten Familien solcher Konfigurationen liefert. Um dies zu klären, leiten wir eine einfache Formel zur Berechnung der Dimension des Lösungsraums für unsere Fragestellung her. Diese sagt für zwei Dimensionen, d.h. bei Platzierung der Atome im zweidimensionalen Raum, die beobachtete, diskrete Lösungsmenge und für drei Dimensionen eine von uns durch die Analyse der die infinitesimale Nachbarschaft einer perfekten Konfiguration beschreibenden Hesse-Matrix bestätigte Anzahl an freien Parametern voraus.

Abstract In this thesis, we investigate perfect transfer of an excitation in networks of 4 to 8 Rydberg atoms via dipole-dipole interaction. We demand that the excitation is transferred between a given pair of an input and an output site with the highest possible efficiency and as fast as possible. Existing experiments motivate a restriction to networks with atoms located on a two-dimensional lattice. We start with an analysis of all possible configurations on lattice sizes accessible with our computational power. In this framework, we do not find any configurations that exhibit 100% transport efficiency. In a second step, we therefore remove the lattice condition and allow the atoms to be placed continuously in two-dimensional space. Indeed, a discrete and finite set of "perfect" configurations, i.e. ones which provide 100% efficiency on short timescales, is found.

As a consequence of this, we ask the question why our numerical optimization results in a set of single perfect configurations, but not in continuous, parameterized families of such configurations. To tackle this problem, we derive a simple formula which predicts the dimension of the space of solutions in our problem. It states that for two dimensions, i.e. if we place the atoms in two-dimensional space, only a discrete set of solutions exists, whereas it yields a certain number of free parameters in three dimensions. These predictions are reproduced with an analysis of the Hessian that describes the infinitesimal neighborhood of a perfect configuration.

Danksagungen

Es gibt viele Gründe, warum ich im Zusammenhang mit dieser Arbeit einigen Personen meinen Dank aussprechen möchte. Am meisten gelernt habe ich von Thomas Wellens, der mit seiner herzlichen Art des Umgangs, den rücksichtsvollen Erklärungen (die er, wenn nötig, nicht müde wurde zu wiederholen) und der durchgehenden Bereitschaft, mir jederzeit spontan mit Rat und Tat zur Seite zu stehen eine Hilfe war, die ich nicht hätte missen wollen. Seine Ideen machen den Kern der theoretischen Ergebnisse dieser Arbeit aus und ermöglichten es mir, meiner Suche eine Struktur zu geben und die Erkenntnisse meiner kurzen Zeit im Arbeitskreis schöner zusammenzufassen, als ich es zwischenzeitlich für möglich gehalten hätte. Andreas Buchleitner gab mir die Möglichkeit, einen Einblick in seine Arbeitsgruppe zu bekommen, worüber ich vor allem deshalb sehr froh bin, weil er es bewerkstelligt hat, sehr besondere Charaktere aus der ganzen Welt an einem Ort zu versammeln. Umgeben von diesen überaus intelligenten und herzlichen Menschen fühlte ich mich durchweg wohl und habe viel gelacht und gelernt.
Danke auch an meine Freunde, die ihr geduldig meinen schon manches Mal nicht zu Ende gedachten Monologen und voreiligen Bedenken ein Ohr leiht. Das bedeutet und hilft mir mehr, als ihr vielleicht denkt. Dies gilt auch für meine ganze, glücklicherweise schon viel gewachsene Familie. Unter ihnen gebührt meinen Eltern jedoch besonderen Dank, denn durch sie lebe ich zu jeder Zeit in der luxuriösen Gewissheit, das machen zu können was ich liebe, während sie mir bei dem zur Seite stehen, das nun einmal sein muss.

Contents

Introduction

Science has been successful in describing a variety of transport processes observed in systems of particles, e.g. diffusion of molecules through a cell membrane, where classical statistical mechanics can be used to obtain an effective, averaged description of the net particle flow. In some situations, only quantum mechanics can provide satisfactory explanations of the underlying dynamics, like the existence of Bloch states in lattices, where the probability of finding an electron is spread over a large region in the crystal. The former only relies on the existence of a concentration gradient, but is not able to describe effects of interference possibly arising for quantum mechanical particles or excitations, while the latter only allows for an analytic solution due to the periodicity of the lattice potential. Interestingly, *unordered* networks of particles exist in nature that feature transport properties which can neither be understood by classical physics, nor by the known analytic solutions of simple quantum mechanical problems. A remarkable example of this is the ability of green sulfur bacteria to transfer an excitation created by an incoming photon from a so-called 'antenna complex' protein to their 'reaction center', where the excitation is converted to chemical energy. To make this possible, the excitation has to be transported very quickly, otherwise the energy is dissipated into the environment and lost for the chemical reaction. This is done by a pigment-protein complex called the *Fenna-Matthews-Olsen complex* [1]. Inside this complex, a disordered network of bacteriochlorophyll-a molecules is embedded loosely into the overall protein structure. Transport of excitations in this network happens with remarkably high efficiency[2] and understanding the behaviour of this network more precisely might enable us to find new ways of thinking about transport of energy, particles and therefore also information. Two of the most prominent possible applications are quantum computing and photovoltaics. Both of them are investigated intensely all over the world, the former to revolutionize our way of performing computations in parallel, the latter to possibly raise the currently available efficiency of solar energy devices, which is indispensable to abolish nonrenewable energy sources and slow down climate change.

Many scientists have engaged in finding an explanation for this phenomenon and a broad range of approaches was created, from models close to experimental data [3], to very abstract descriptions of transport processes in general [4]. These coexisting models tend to disagree in basic assumptions. One example is the question whether a coherent superposition of states is responsible for the high transfer probabilities or whether the ambient noise enhances transport. In 2007, evidence in favour of a coherent transport mechanism inside the FMO complex has been found [5]. Coherence seems to persist in these networks for longer timescales than expected, although thermal noise at ambient temperatures and coupling of the individual two-level systems inside the complex to the surrounding structure should in principle suppress coherent state transfer. Should we find a way to mimic this robustness, this would bring us much

closer to the aforementioned applications. Unfortunately, the modelling of the complicated dynamics inside the complex remains difficult.

Therefore, we have to think of systems that preserve the essential characteristics of the networks implemented in nature, but which at the same time are simple enough to allow for a successful analysis. Rydberg atoms, which exhibit one electron in a highly excited state, are a way of controlling networks of two-level systems interacting via electric dipole-dipole interactions in reality and investigate their behaviour, e.g. under introduction of an additional excitation into the system [6]. In this thesis, we model purely coherent transfer of one single excitation entering a 2D network of Rydberg atoms. We are especially interested in configurations that provide fast and highly efficient excitation transport from a given input to a given output site. The thesis will be structured in the following way:

- *Chapter 1*: A description of the underlying model and the definition of a measure for transfer efficiency is given.

- *Chapter 2*: We fix the position of atoms on a discrete, two-dimensional lattice. This is motivated by existing experimental setups [7]. Allowing between 4 and 8 atoms on the lattice, we identify configurations exhibiting transport efficiencies up to 99.99%, but we do not reach unity.

- *Chapter 3*: As an extension, we remove the condition imposed in chapter 2 and sample continuously distributed configurations of 4 to 7 atoms in the unit disk, to which we apply methods of numerical optimization. The resulting sets of optimal configurations are discrete (meaning every configuration is isolated in space), feature perfect transfer efficiency and the minimal transfer time is shortened for every additional site in the network, up to a factor of 30 times faster than a Rabi oscillation between the two most distant sites only.

- *Chapter 4*: We show that our results are consistent with earlier work in the field and use the criteria and ideas from these sources to derive a simple criterion which allows us to understand why only discrete sets of configurations appear in two dimensions. Additionally, it enables us to predict a number of free parameters that one can vary for perfect configurations in three dimensions without decreasing the efficiency.

- *Chapter 5*: An approximation of the efficiency function around perfect configurations up to second order results in a Hessian matrix. By evaluating the number of its zero eigenvalues, we confirm our predictions of chapter 4.

Chapter 1

Model and Definition of Transfer Efficiency

1.1 Model

The networks we are interested in consist of at least 4 sites which we use to model the individual Rydberg atoms, where the atoms with the largest distance to each other are fixed in position and called the *input (in)* and *output (out)* site, respectively. All remaining atoms lie in between these two and can either be put on a square lattice or continuously distributed in the unit disk with the line from *in* to *out* defining the diameter. In both cases, we use the scale invariance of the problem and set the distance of *in* to *out* to a fixed value of 2. Therefore, increasing the lattice size approximates the continuous case to a better and better degree.

We assume pure electric dipole-dipole interaction between the atoms and set their absolute potential (on-site) energies to zero, using the fact that a constant energy shift on the diagonal elements of the Hamiltonian does not influence the dynamics of the system. We model the Rydberg atoms with one outer electron excited to a Rydberg state with a high principal quantum number n. It can be in a lower or upper Rydberg state denoted by $|S\rangle \equiv |n\,S_{1/2,1/2}\rangle$ and $|P\rangle \equiv |n\,P_{3/2,3/2}\rangle$, respectively. S and P refer to orbital angular momentum $l = 0$ and $l = 1$ of the excited electron and the half integers in subscript are the quantum numbers of total angular momentum j and its projection onto the z-axis m_j. In the case of rubidium atoms for example, $n = 46$ is an adequate choice [8].

We only look at the situation where one single excitation is in the system. The state of the system at time t is then written as $|\psi(t)\rangle$ and for the excitation fully localized at site i, this will be denoted by $|i\rangle$, where $|in\rangle = |1\rangle$ and $|out\rangle = |k\rangle$ for a number of atoms k. As an example we can write the initial state, where the excitation is fully localized at site *in*, as

$$|\psi(0)\rangle = |1\rangle = |P\rangle_1 \otimes |S\rangle_2 \otimes \cdots \otimes |S\rangle_k.$$

The entirety of all states $|i\rangle,\ i \in 1, ..., k$ forms a basis of the single-excitation Hilbert space $\mathcal{H}$. The coupling strengths between atom i and j, which as Rydberg atoms are electric dipoles with orientation chosen to be along the laboratory's z-axis, are given by

$$V(\vec{r}_{ij}) = \frac{\alpha}{r_{ij}^3} \cdot (3\cos^2(\theta) - 1), \tag{1.1}$$

where α is a constant depending on the dipole moments between the states $|S\rangle$ and $|P\rangle$. θ is the angle between the laboratory's z-axis and the vector $\vec{r}_{ij}$ connecting site i and j. r_{ij} is its

absolute value [8]. In our case, since a reduction to a two-dimensional setting is performed, $\theta = \pi/2$ for all cases, given the laboratory's z-axis is perpendicular to the plane in which positions can be varied. It remains a dependence on r^{-3}, where the proportionality factor can be ignored by rescaling energies, including $\hbar = 1$. Since a constant factor is not influencing the dynamics, we can also ignore the minus sign and obtain a very simple expression for the entries of the Hamiltonian

$$H_{ij} = \begin{cases} V_{ij} = \dfrac{1}{r_{ij}^3} & i \neq j \\ 0 & i = j \end{cases} \tag{1.2}$$

Kinetic energy due to atomic motion does not appear because we fix the atoms at their positions. The Hamiltonian is symmetric and has real entries, so we know the eigenvectors will form an orthogonal basis in $\mathcal{H}$.

1.2   Transfer Efficiency

Our ultimate goal is to search for configurations that exhibit very high transport efficiency. Different ways of assessing this efficiency are at our disposal as explained in [9]. One can either examine the maximum probability of the excitation being localized at the output site at any given point in an arbitrarily chosen time interval, or its time average over the latter, where a unitary time-evolution of the state vectors in the single excitation Hilbert space is used. There exists an additional possibility that does not rely on pure states but instead uses a Markovian master equation and Lindblad terms to model a 'sink' at the output site, but we will not pursue this approach for reasons of simplicity. Given that we are looking for completely perfect transport, the maximum probability measure seems to be the most reasonable option. The mean value for long times can not exceed 50% which is just the case of *in* and *out* exchanging the excitation without any intermediate sites.

As an additional condition to unit efficiency, we demand transfer times $t < T$, where T is a certain fraction of the period $T_{Rabi} = \pi/(2\,V_{1k})$ of a Rabi oscillation between *in* and *out*, which are coupled by $V_{1k} = 1/8$. The intermediate sites can not only drastically enhance or suppress transport in general but also speed it up by a large factor. The purpose of our chosen benchmark time is therefore to prefer configurations that reach high transport efficiencies in a time smaller than T_{Rabi}. We vary the allowed value of T depending on the situation, always minimizing it as far as possible. We then find for the probability $\mathcal{P}(T)$ of the excitation to be localized at site *out* at any time smaller than T

$$\mathcal{P}(T) = \max_{t \in (0,T)} |\langle k|\psi(t)\rangle|^2 = \max_{t \in (0,T)} \left|\langle k| e^{-iHt} |1\rangle\right|^2, \tag{1.3}$$

where we used the time evolution operator for the time-independent Hamiltonian. Taking advantage of the fact that we know the eigenvectors of H form an orthogonal basis, we can calculate and normalize it to $\{|v_i\rangle\}$. This allows us to explicitly evaluate the matrix exponential and insert the spectral decomposition of H in Eq.(1.3):

$$\mathcal{P}(T) = \max_{t \in (0,T)} \left| \sum_j e^{-iE_j t} \langle k|v_j\rangle \langle v_j|1\rangle \right|^2. \tag{1.4}$$

This quantity has been assessed numerically for all configurations in this thesis. Note that, due to the fact that all matrix elements of H are real numbers, the transfer efficiency is symmetric under exchange of the input and output site:

$$\langle k| \, e^{-iHt} \, |1\rangle^* = \langle 1| \, (e^{-iHt})^\dagger \, |k\rangle^* = \langle 1| \, e^{iHt} \, |k\rangle^* = \langle 1| \, e^{-iH^*t} \, |k\rangle = \langle 1| \, e^{-iHt} \, |k\rangle \quad (1.5)$$

The important assumption in our model, namely that Rydberg atoms are fixed to well controlled positions, may not be easily implementable in experiments. Optical lattices, where laser light creates periodic potentials in which neutral atoms can be trapped, are one way to solve this issue. This technology has succeeded not only in creating large, two-dimensional arrays where Rydberg atoms can be fixed in space, but also in creating potential wells that are sufficiently narrow so that we can neglect the atoms' motion due to the uncertainty relation, which is explained in detail in [7].

Chapter 2

Optimal Transfer on 2D Lattices

In general, the transfer efficiency defined by Eq. (1.4) sensitively depends on the atomic positions [10]. In this chapter, we will search optimal configurations of atoms on a two-dimensional lattice which maximize $\mathcal{P}$. For this purpose, we choose $N \times N$ lattices with odd N, where *in* and *out* lie in the center of opposing edges.

2.1 Range of Calculations

The transfer efficiencies $\mathcal{P}(T)$, see Eq.(1.4), for all configurations of at least four and up to 8 atoms on lattices of size $N = 5$ or larger have been calculated for the benchmark times $T = T_{Rabi}/10$ and $T = T_{Rabi}/5$. Given the fixed positions of *in* and *out*, a number of atoms k and a lattice with N^2 positions, this results in $\binom{N^2-2}{k-2}$ possibilities for configurations. For our values of k and N, this number grows rapidly in size as both of them are increased, so in terms of computational power a surprisingly limited set of combinations of the two parameters could be considered. Intuitively, one could argue that a further optimization of these calculations could be possible by focusing the search on configurations with certain symmetry properties, thus enabling us to examine larger grids in the same computation time. In this case though, we would have to justify why symmetry should be a preferred feature for candidate configurations. We will be addressing this at a later point based on the results for all possibilities on small lattices.

2.2   Results

We gathered the efficiencies of the best performing configurations for each case in Table 2.1 $(T = T_{Rabi}/10)$ and 2.2 $(T = T_{Rabi}/5)$. The corresponding times for which maximal efficiency is reached are presented in the appendix under 5.11 and 5.12.

N $\times$ N	4	5	6	7	8
5x5	0.33440	0.88839	0.86716	0.91202	0.95321
7x7	0.91544	0.85755	0.94245	0.95528	0.97692
9x9	0.74015	0.94833	0.94457		
11x11	0.77268	0.94821	0.97508		
13x13	0.92139	0.93763			

Table 2.1: Maximal efficiencies $\mathcal{P}(T)$ for lattice sizes N between 5 and 13 with $4-8$ atoms, where $T = 0.1 \cdot T_{Rabi}$

N $\times$ N	4	5	6	7	8
5x5	0.78572	0.98073	0.87671	0.96177	0.95321
7x7	0.91544	0.99709	0.99488	0.99730	0.99393
9x9	0.86775	0.99668	0.99651		
11x11	0.85326	0.99954	0.99993		
13x13	0.92139	0.99709			

Table 2.2: Maximal efficiencies $\mathcal{P}(T)$ for lattice sizes N between 5 and 13 with $4-8$ atoms, where $T = 0.2 \cdot T_{Rabi}$

We can see that for $t < T_{Rabi}/10$, the maximal efficiencies gather mostly around 95% and do not reach more than 97.7%. With a few exceptions, there exists a general trend for them to rise as the number of atoms on a fixed lattice size is increased.

Although 3 out of 5 lattice sizes for configurations with $k = 4$ atoms do not display very efficient possibilities, surprisingly the 7×7 and 13×13 lattices do. Figure 2.2 shows both of them as (almost) one dimensional, symmetric arrangements with (nearly) equidistant atoms. In general, the increase in T results in a drastic improvement of transport, where in all of the cases of 5 or more atoms on a 7×7 or larger grid, unity is reached within less than 1% deviation.
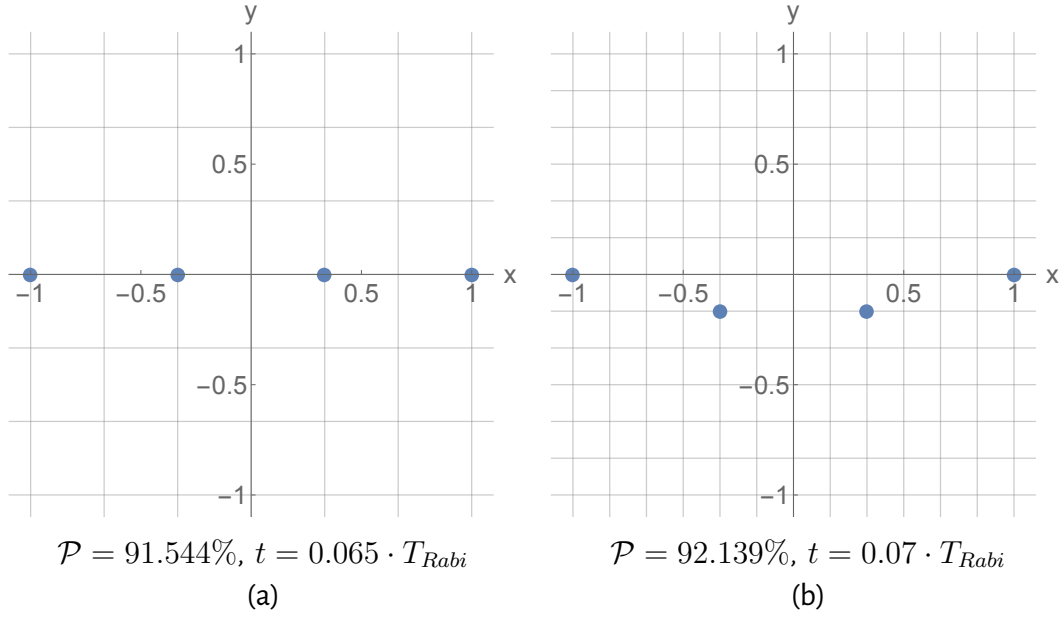
$$\mathcal{P} = 91.544\%,\ t = 0.065 \cdot T_{Rabi}$$

(a)

$$\mathcal{P} = 92.139\%,\ t = 0.07 \cdot T_{Rabi}$$

(b)

Figure 2.1: Optimal configurations of 4 atoms on the 7×7 (a) and 13×13 (b) lattice. Both configurations are optimal for both benchmark times $T = 0.1 \cdot T_{Rabi}$ and $T = 0.2 \cdot T_{Rabi}$

As the best performing configurations for 5, 6 and 7 atoms demonstrate below, see Figs. 2.2-2.4, spatial symmetry is not a necessary condition for optimal transport. It is therefore a priori *not* reasonable to restrict the search only to symmetric configurations.

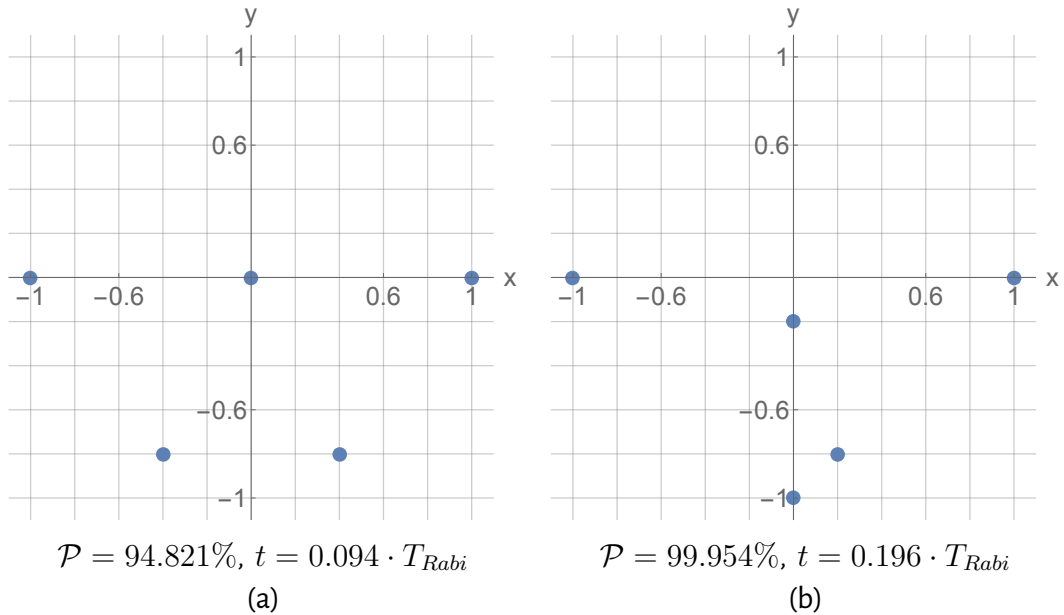$$\mathcal{P} = 94.821\%,\ t = 0.094 \cdot T_{Rabi}$$

(a)

$$\mathcal{P} = 99.954\%,\ t = 0.196 \cdot T_{Rabi}$$

(b)

Figure 2.2: Optimal configurations of 5 atoms on the 11×11 lattice for $T = 0.1 \cdot T_{Rabi}$ (a) and $T = 0.2 \cdot T_{Rabi}$ (b)

$$\mathcal{P} = 97.508\%,\ t = 0.092 \cdot T_{Rabi}$$

(a)

$$\mathcal{P} = 99.993\%,\ t = 0.185 \cdot T_{Rabi}$$

(b)

Figure 2.3: Optimal configurations of 6 atoms on the 11×11 lattice for $T = 0.1 \cdot T_{Rabi}$ (a) and $T = 0.2 \cdot T_{Rabi}$ (b)

$$\mathcal{P} = 95.528\%,\ t = 0.082 \cdot T_{Rabi}$$
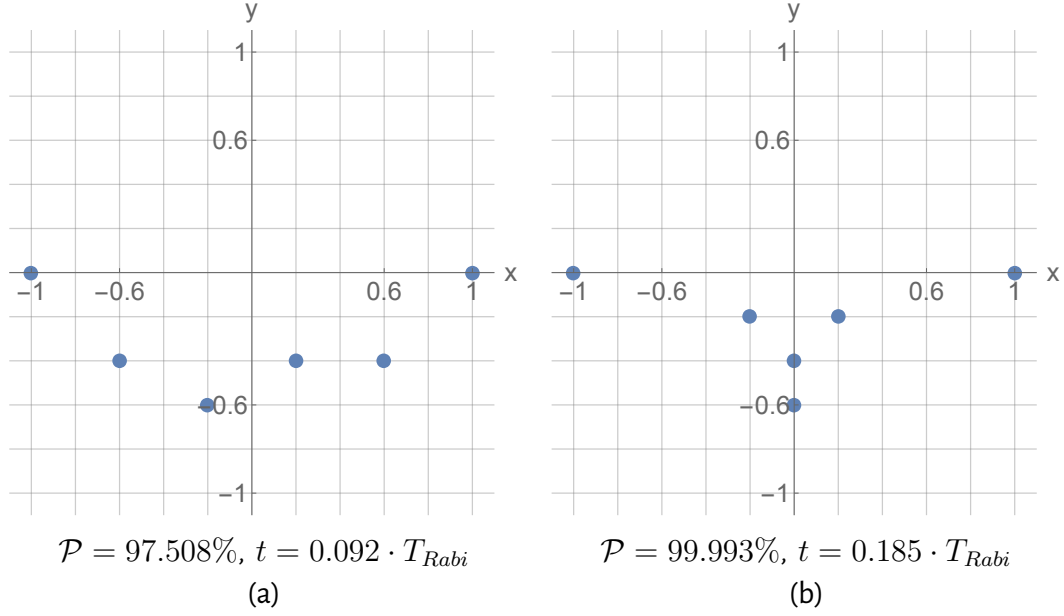
(a)

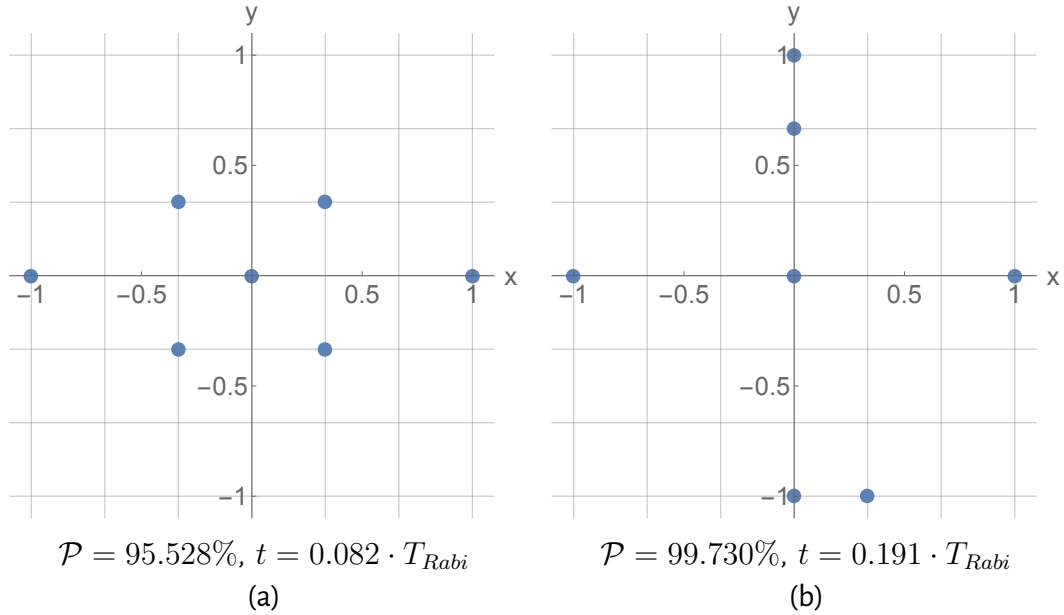$$\mathcal{P} = 99.730\%,\ t = 0.191 \cdot T_{Rabi}$$

(b)

Figure 2.4: Optimal configurations of 7 atoms on the 7×7 lattice for $T = 0.1 \cdot T_{Rabi}$ (a) and $T = 0.2 \cdot T_{Rabi}$ (b)

Obviously, these observations can only give us a first hint about the nature of the perfect transfer we are searching for. Nevertheless, they already provide candidates that reach almost perfect transfer with less than one percent deviation from unity, which might well lie inside experimental error margins anyway, while reducing the transfer time by a factor of five, and even by a factor of ten if one is willing to decrease the efficiency to 97.5%.

Apart from that, however, the method applied does not provide any further insight, since the calculations on discrete lattices becomes difficult too quickly. We will therefore vary our approach in the next chapter and allow the atoms to be placed at arbitrary positions inside the unit disk.

Chapter 3

Perfect Transfer in Arbitrary 2D Networks

From previous work, it is known that certain configurations reach perfect transfer ($\mathcal{P} = 1$) in three dimensions [10, 11]. In this chapter, we check whether perfect and fast transfer (where $T \ll T_{Rabi}$) is possible in two dimensions, if the atoms are allowed to be placed at arbitrary positions, and present an overview of the set of optimal configurations achievable for a number of atoms between 4 and 7.

3.1   Numerical Optimization Algorithm

The results have been obtained by

- sampling configurations with a pseudo-random number generator

- improving these with the help of a simple genetic algorithm [9]

- further optimizing the obtained configurations with a simplex method [12]

This combination of algorithms proved to be the most effective one, since for inefficient sample configurations, the simplex method is slightly less convergent than for the ones near 100% efficiency. The genetic algorithm applies random variations to the coordinates of all intermediate sites, where the magnitude of variation decreases the closer the efficiency is to unity. The changes are saved if any improvement is obtained and the procedure is iterated. In contrast, the simplex method is an analytical optimization algorithm where only the initial parameters are chosen randomly. Combining these two provides a good tool to quickly find configurations that exhibit efficiencies very close to one. In the whole process, only realizations with pairwise atomic distances of $d \geq 0.1$ have been accepted, what resulted in an upper bound for the interaction between each pair of atoms. It has been shown that sites lying very close to each other prevent spreading of states in the network and the minimal distance is implemented to avoid such a detrimental effect, which has been called *pair localization* in [8]. For the continuous setting, a minimum efficiency of $P_{min} = 1 - 10^{-13}$ was demanded in all cases except for 4 atoms, where probabilities from $\mathcal{P}_{min,4} = 1 - 10^{-6}$ upward were allowed. This is explained in further detail below and is due the fact that only for $k = 4$ the overall structure does not change significantly from $\mathcal{P}_{min,4}$ on. For higher numbers of atoms though,

the distribution of positions continues to decrease with higher thresholds, so it was desirable to make the condition as strict as possible and to focus on regularities that persist. In the appendix, we present corresponding graphs where we chose $\mathcal{P}_{min,4}$ for $k \geq 5$ instead, and show that the resulting difference is indeed remarkable.

The maximal allowed transfer time was set to $T = 0.5 \cdot T_{Rabi}$ for $k = 4$. For all following searches, we determined the fastest configuration of the previous atom number and used its transfer time to set a new upper limit. This way, we restrict ourselves to configurations where the additional atom actually improves the speed of transport.

3.2 Perfect Configurations: Overview

In Fig. 3.1 we plotted all found configurations of 4 atoms exhibiting perfect excitation transfer. We can see 4·27 + 2· 5=118 points corresponding to 59 pairs of intermediate sites. As we have checked, all of them are either symmetric with respect to the origin or with respect to the y-axis. As an example, we show in Fig. 3.2 the two fastest ones among all the configurations shown in Fig. 3.1. Both are symmetric with respect to the origin. Moreover, they are mirror-symmetric counterparts of each other and therefore (due to the symmetry of H under exchange of *in* and *out*, see 1.2) exhibit exactly the same transfer time. If we count symmetric counterparts (such as the ones shown in 3.2) as only one configuration, we arrive at 27+5=32 different configurations, shown in Fig. 3.1. 5 of them are located on the y-axis, and are symmetric with respect to the origin and both axes.
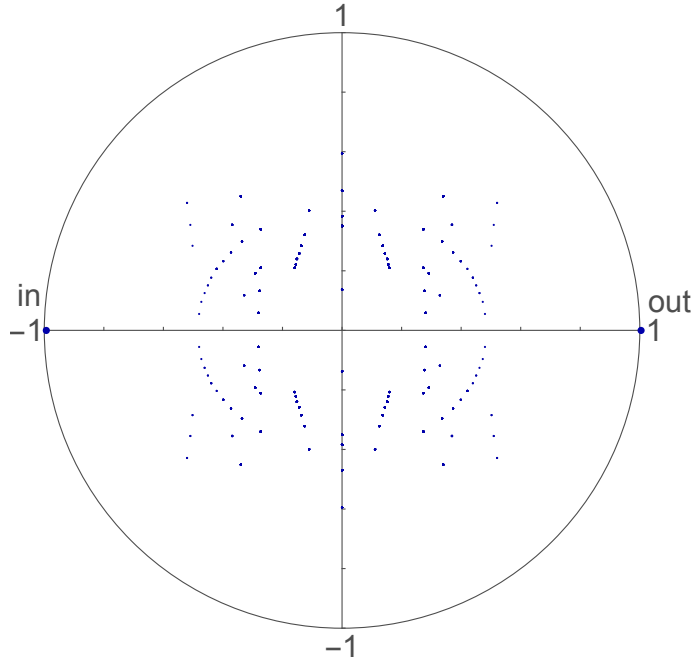

Figure 3.1: Set of perfect configurations with 4 atoms, where $T < 0.5 \cdot T_{Rabi}$. The input and output atom are fixed at positions (-1,0) and (1,0), each dot inside the disk represents one atom of a perfect configuration.
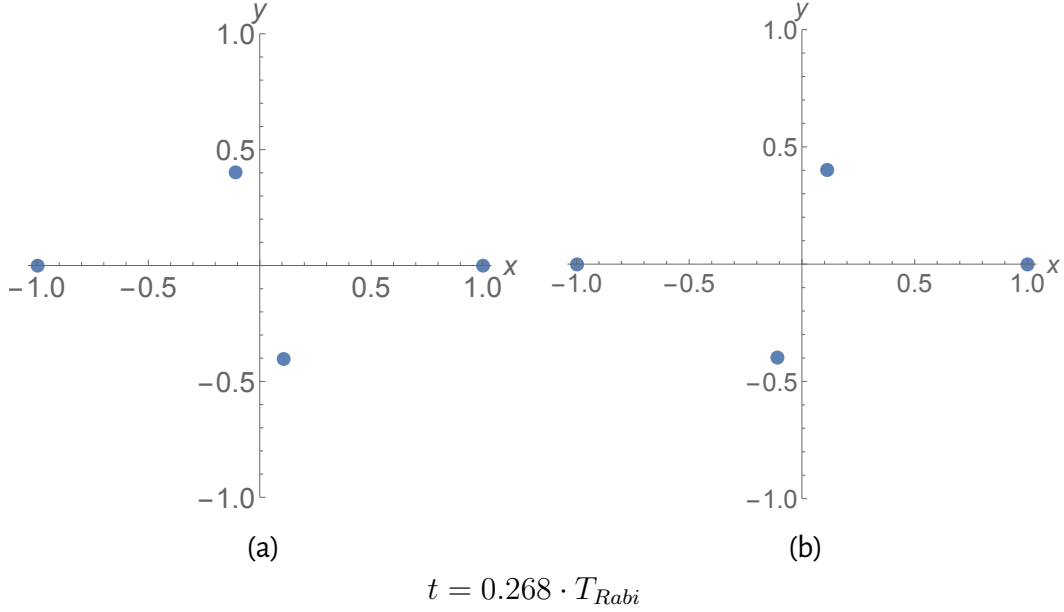
$$t = 0.268 \cdot T_{Rabi}$$

Figure 3.2: The two possible arrangements of the fastest optimal configuration with 4 atoms. Both of them are symmetric to the origin and exhibit the same transfer time.

For $k = 5$ atoms, we found, both, symmetric and asymmetric configurations with efficiency $\mathcal{P} = 1$. Fig. 3.3 shows the ensemble pictures for asymmetric and symmetric configurations separately. The fastest transfer time observed with $k = 4$, see 3.2, was used to set $T = 0.268 \cdot T_{Rabi}$. In the symmetric case (b) it is not surprising to find a high density of atoms along the y-axis, since it is required for any configuration of an uneven number of atoms that is symmetric to have one atom on it. The consequence of this is more interesting. Because there is always one atom with x-coordinate zero, a 'forbidden' zone appears for $|x| \lesssim 0.24$. This is likely due to the pair localization effects we mentioned above. Since a suppression of transport takes place if the other two atoms are too close to the one located in the center, we do not see these configurations in our analysis. We count 14 sites in one quadrant (not including the sites along the y-axis). All of these configurations are symmetric with respect to the y-axis, so we can say there exist 14 distinct symmetric configurations, each of which exhibits one counterpart obtained by mirroring with respect to the x-axis.

In contrast, Fig. 3.3 (a) only shows 9 sites in one quadrant. This leads to 36 sites altogether and therefore with 3 intermediate atoms to 12 arrangements, if we assume that none of them share the same site. Since no symmetry exists in these cases (the symmetry of the ensemble only appears because we can mirror the asymmetric configurations about the x- and y-axis, creating a symmetric image out of the 4 possibilities for each asymmetric configuration) we end up with 12/4=3 different configurations. We show the two slower ones in 3.4, whereas the fastest one is presented in 3.7. In total, we found a set of 17 new configurations that actually perform better than 4 atom networks, which is again a surprisingly small number.

The graphics in Fig. 3.3 share an important feature: The vicinity of *in* and *out* is not populated: A minimal distance to the intermediate sites of at least 25% compared to their own separation is always observed. This result is consistent with the observations in [13], where the concepts of centrosymmetry and the dominant doublet presented in section 4.1 have been used to explain the phenomenon.
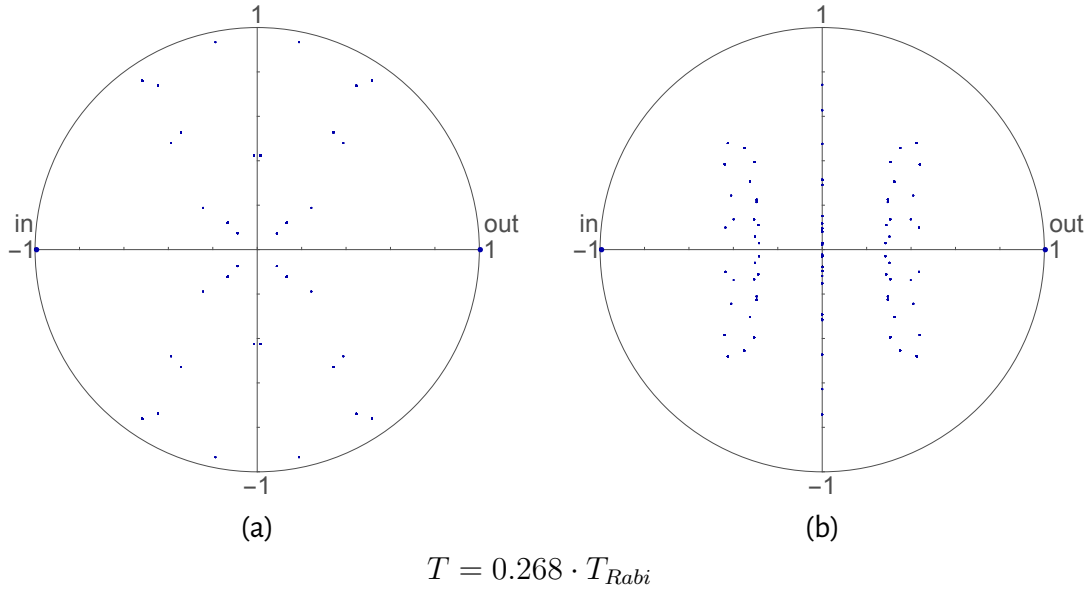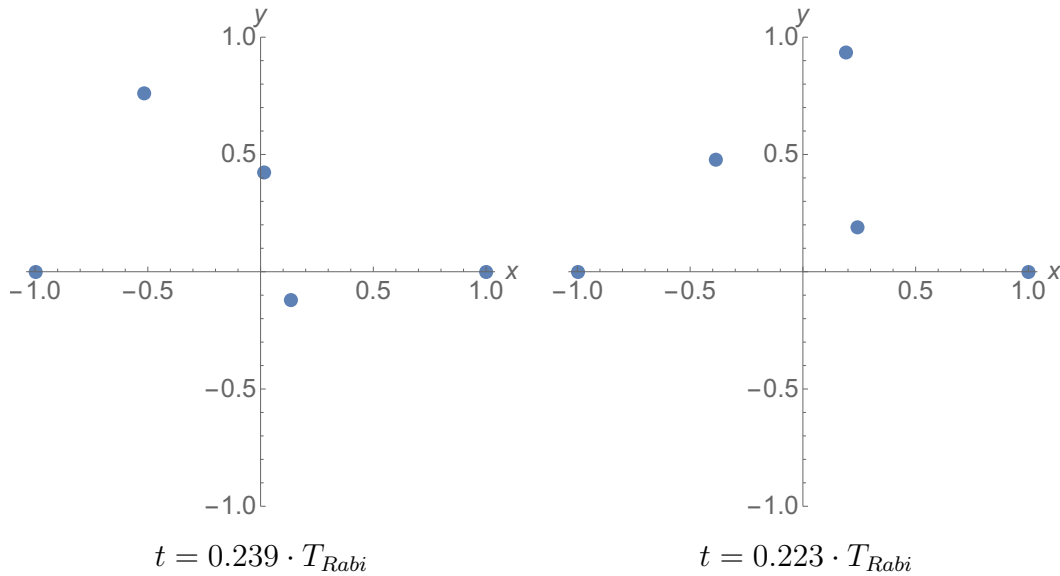
$$T = 0.268 \cdot T_{Rabi}$$

Figure 3.3: Ensembles of asymmetric (a) and symmetric (b) optimal configurations with 5 atoms

$$t = 0.239 \cdot T_{Rabi} \qquad\qquad t = 0.223 \cdot T_{Rabi}$$

Figure 3.4: Two of the three distinct optimal configurations appearing in 3.3 (a). The third one, shown in 3.7, is the fastest asymmetric configuration we found for $k = 5$.

For 6 atoms, we again see the empty regions near *in* and *out* with radii comparable to the ones in Fig. 3.3 (and incidentally also Fig. 3.1) as well as approximately 60 configurations (where we applied similar arguments to the ones above). As a close inspection of the ensembles represented in Fig. 3.5 (a) and (b) reveals, they are not completely symmetric anymore, which indicates that some configurations have not been found. Fig. 3.5 was generated with the data obtained from 1700 runs of the optimization algorithm, and more runs would be needed to find all configurations (including all their symmetric counterparts).

Nevertheless, our data clearly indicates that the configurations of interest form a discrete set in the case of $k = 6$ also.

$$T = 0.113 \cdot T_{Rabi}$$
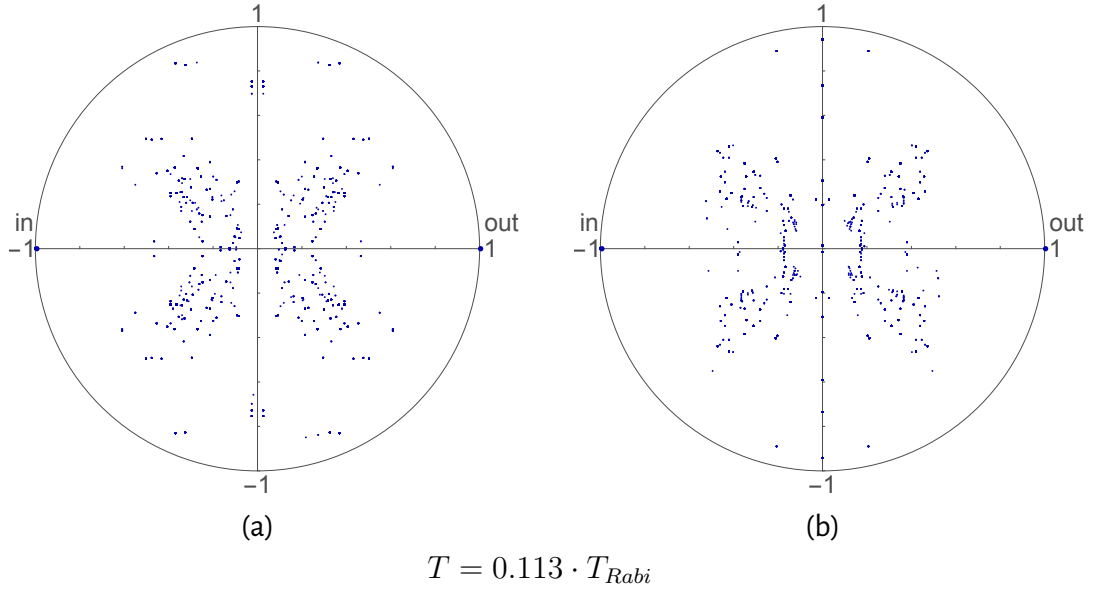
Figure 3.5: Ensembles of asymmetric (a) and symmetric (b) optimal configurations with 6 sites

$$T = 0.071 \cdot T_{Rabi}$$
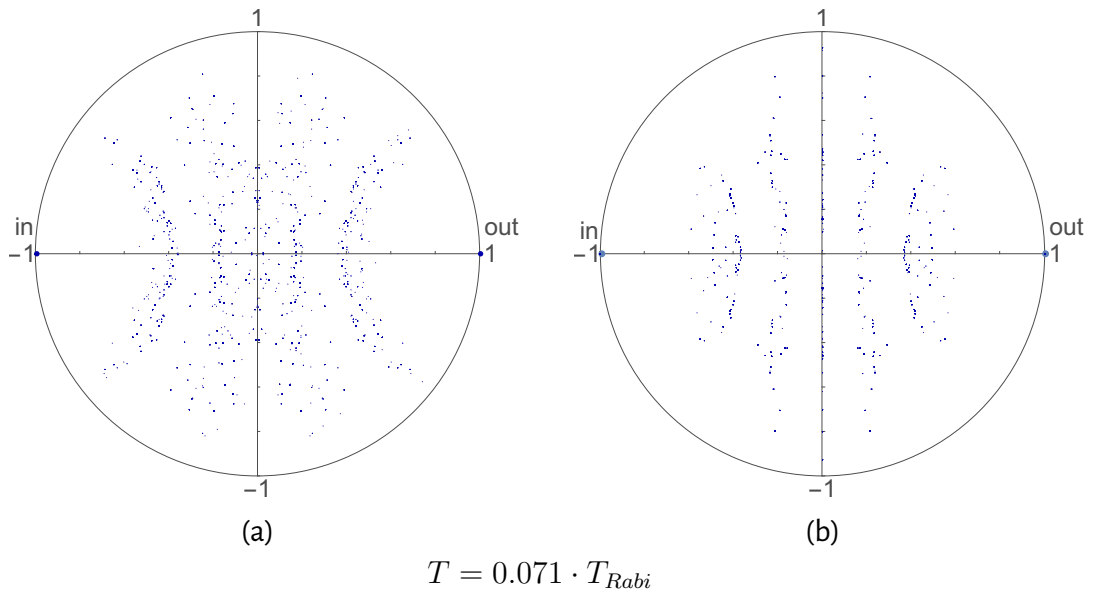
Figure 3.6: Ensembles of asymmetric (a) and symmetric (b) optimal configurations with 7 atoms

For $k = 7$, we observe the same features in Fig. 3.6 as we did for 6 atoms. The radial minimal distance of all intermediate sites to *in* and *out* is clearly visible, especially in the asymmetric ensemble picture. The number of distinct configurations has increased to approximately 90 (where again, not all of them might have been found by our algorithm with 1700 runs), meaning we get more and more options to enhance transport compared to smaller atom numbers.

3.3 Individual Examples for Fastest Transfer

In Fig. 3.2 and 3.7 to 3.9, the fastest asymmetric and the fastest symmetric configuration for the respective number of atoms is displayed. While all of them exhibit perfect state transfer, the symmetric configurations provide faster transport in each case. As explained above, their values are the transfer times used as benchmark for the overview pictures with larger numbers of atoms. Naturally, one would wonder whether there is a general dependence of transfer time on the presence of symmetry in a configuration.

To make more general statements about this, one would have to perform a thorough analysis of types by accepting each configuration type only once. In our procedure used to generate the above ensembles, we allowed configurations to enter a sample as many times as they occur by chance. To avoid this, one would have to apply a certain criterion for which kind of configuration is equal to another one and take into account the possible symmetries and permutations of atoms when deciding whether a particular set of atoms has already been observed. With the dataset obtained in such a fashion, a differentiation between symmetric and asymmetric configurations could then lead to an observable difference in transfer time properties. Unfortunately, we did not have enough time to tackle this interesting question appropriately.

All coordinates of the configurations displayed in Fig. 3.2, 3.7, 3.8 and 3.9 have been listed in appendix C.

$$(a)$$
$$t = 0.210 \cdot T_{Rabi}$$

$$(b)$$
$$t = 0.113 \cdot T_{Rabi}$$
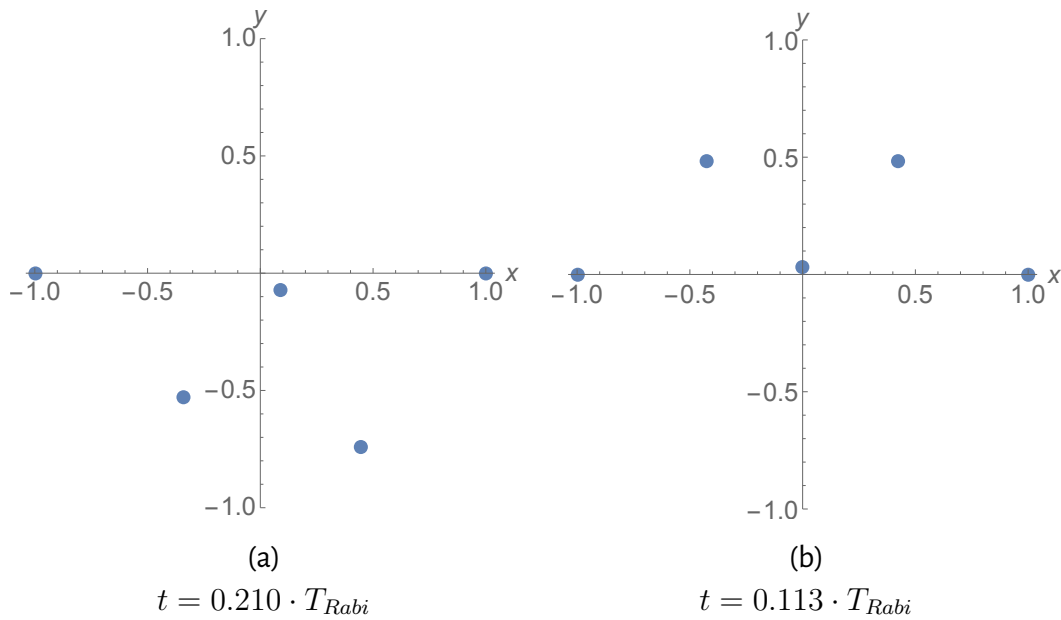
Figure 3.7: The fastest asymmetric (a) and symmetric (b) optimal configuration with 5 atoms

$$t = 0.070 \cdot T_{Rabi} \qquad\qquad t = 0.054 \cdot T_{Rabi}$$
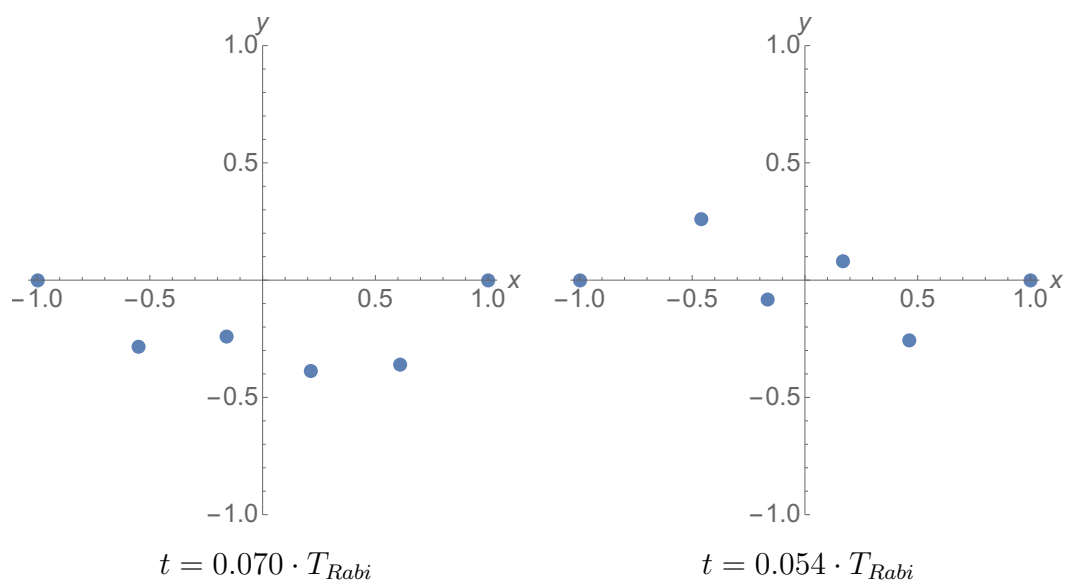
Figure 3.8: The fastest optimal asymmetric (a) and symmetric (b) configuration with 6 atoms

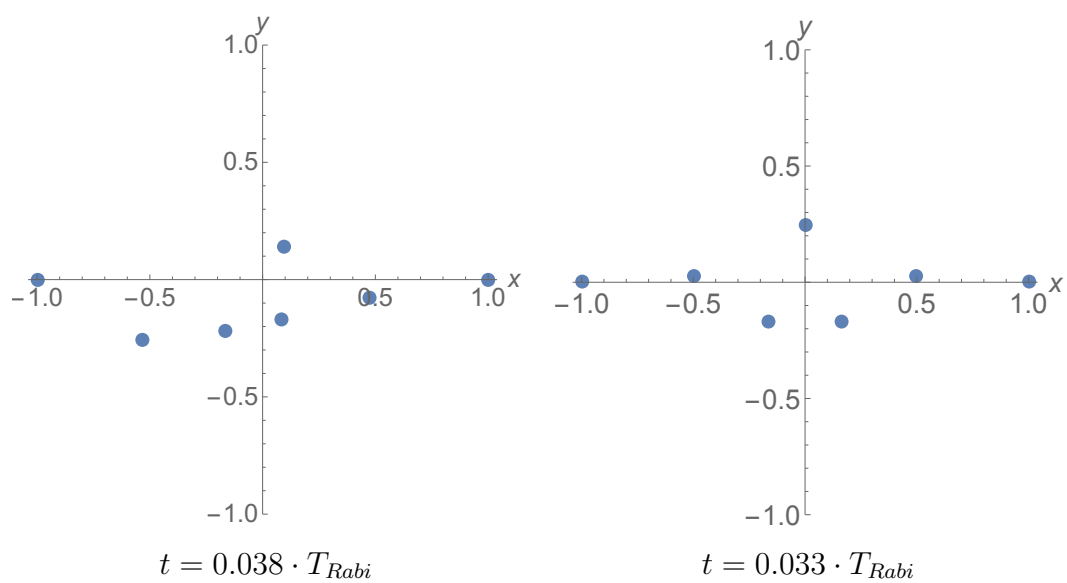$$t = 0.038 \cdot T_{Rabi} \qquad\qquad t = 0.033 \cdot T_{Rabi}$$

Figure 3.9: The fastest asymmetric (a) and symmetric (b) optimal configuration with 7 atoms

Chapter 4

Conditions for Perfect Transfer

In the previous chapter, we found sets of configurations that provide perfect state transfer. Since we set an upper limit for the allowed transfer time, the sets were finite and, due to our restriction of improvement with each additional atom, quite small.

After this phenomenological approach, we want to understand the results analytically by deriving necessary *and* sufficient conditions for perfect state transfer. We then move on to compare the number of independent conditions we can find with the number of parameters that are available for a configuration in d dimensions and a network of k atoms.

4.1   Centrosymmetry and Dominant doublet

In previous work, the combination of two specific design principles has been associated with highly efficient and fast state transfer [13, 14]. The first one is the so-called *centrosymmetry*. A Hamiltonian is called centrosymmetric if it commutes with the permutation operator $\hat{P}$ that is represented by the exchange matrix $J = \delta_{i,k-j+1}$, so

$$HJ = JH \quad \Rightarrow \quad H_{i,j} = H_{i,\,k-j+1} = H_{k-i+1,j} \;, \tag{4.1}$$

$$J^2 = \mathbb{1} \quad \Rightarrow \quad H = JHJ^{-1} \;\Rightarrow H_{i,j} = H_{k-i+1,k-j+1} \;. \tag{4.2}$$

which means the Hamiltonian is symmetric about the antidiagonal in addition to being a symmetric matrix.

The second design principle is the *dominant tunneling doublet* or simply dominant doublet. Since centrosymmetric Hamiltonians commute with J, they can be cast into a block diagonal form in the eigenbasis of J with the blocks H^+ and H^- associated with eigenvalues ± 1 of J.

$$H = \begin{bmatrix} H^+ & 0 \\ 0 & H^- \end{bmatrix} . \tag{4.3}$$

H has eigenstates $|\widetilde{\pm}\rangle$ belonging solely to the respective one of these two matrices. J, in turn, has eigenvectors which are symmetric or antisymmetric to the exchange of *in* and *out*, e.g. $|\pm\rangle = (1/\sqrt{2})(|in\rangle \pm |out\rangle)$. If the overlaps fulfill the condition

$$\left| \langle \widetilde{\pm} | \pm \rangle \right|^2 > \alpha \approx 1, \tag{4.4}$$

then $|\pm\rangle$ is said to be a dominant doublet for the Hamiltonian. In [13, 14] it is shown that in general, a dominant doublet exists if the coupling of *in* and *out* to the intermediate sites is small compared to the coupling between the latter. The transfer efficiency for Hamiltonians with both centrosymmetry and a dominant doublet as a property is on average drastically increased compared to randomly sampled Hamiltonians. Nevertheless, configurations that exhibit both properties are not necessarily highly efficient in every case. To actually guarantee that the transfer efficiency reaches unity for a given configuration, additional conditions have to be met.

4.2 Necessary and Sufficient Conditions for Unit Efficiency

We start from the derivations made in [9], where necessary conditions for perfect transfer in the range of the used model have been found.

Starting from Eq.(1.4), the triangle inequality as well as the Cauchy-Schwarz inequality are applied:

$$
\begin{aligned}
\mathcal{P} &= \left| \sum_j e^{-iE_j t} \langle k|v_j\rangle \langle v_j|1\rangle \right|^2 \leq \left(\sum_j |\langle k|v_j\rangle \langle v_j|1\rangle| \right)^2 \\
&\leq \underbrace{\sum_i |\langle k|v_i\rangle|^2}_{1} \underbrace{\sum_l |\langle k|v_l\rangle|^2}_{1} = 1,
\end{aligned}
\tag{4.5}
$$

Of course, the interesting case is equality, which can be reached by demanding

$$
|\langle 1|v_j\rangle|^2 = |\langle k|v_j\rangle|^2 \qquad\qquad j = 1, \ldots, k
\tag{4.6}
$$

for the Cauchy-Schwarz inequality. In addition, if all phases acquired by each term in Eq.(4.5) during the time evolution are equal to an arbitrary phase ϕ modulo 2π at some time t, we achieve equality for the triangle estimate, too:

$$
\arg(e^{-iE_j t} \langle k|v_j\rangle \langle v_j|1\rangle) = \phi \qquad j = 1, \ldots, k
\tag{4.7}
$$

One can show that centrosymmetry is sufficient to guarantee Eq.(4.6): Centrosymmetric Hamiltonians commute with J, so they share a set of eigenvectors with the permutation operator. J only has eigenvalues ± 1, and since it exchanges *in* and *out*, the first and last coefficient of each vector has to be of equal absolute value, which is exactly what Eq.(4.6) states. In general though, there might also exist Hamiltonians that fulfill the conditions without being centrosymmetric. Therefore we have to identify the exact number of independent equations we obtain from Eq.(4.6) and Eq.(4.7). In principle, both of them yield k equations, but these numbers are reduced:

· The eigenvectors of H as well as the excitation position vectors form an orthonormal basis. This implies $\langle 1|1\rangle = \langle k|k\rangle = 1$ and $\sum_{i=1}^{k} |v_i\rangle \langle v_i| = \mathbb{1}$, which results in

$$
\sum_{i=1}^{k} |\langle 1|v_i\rangle|^2 = \sum_{i=1}^{k} |\langle k|v_i\rangle|^2 = 1.
\tag{4.8}
$$

· All diagonal elements of H in the position basis are equal, in our case zero. If we express the Hamiltonian in spectral form $H = \sum_{i=1}^{k} E_i \ket{v_i} \bra{v_i}$ and represent it in the position basis, it must be true that $\bra{1} H \ket{1} = \bra{k} H \ket{k}$, leading to

$$\sum_{i=1}^{k} E_i \left| \braket{1|v_i} \right|^2 = \sum_{i=1}^{k} E_i \left| \braket{k|v_i} \right|^2 = 0. \tag{4.9}$$

These two equations reduce the number of conditions we have to fulfill to $k - 2$, which means if $k - 2$ eigenvectors have the property (4.6), then Eq.(4.8) and Eq.(4.9) guarantee that the remaining two also have it.

The additional constraints on the relative phases give us an additional set of $k - 1$ equations. The phase of one of the terms in Eq.(4.7) is an arbitrary choice, the remaining ones to have be equal to it modulo 2π.

In total, we find

$$c = k - 2 + k - 1 = 2k - 3 \tag{4.10}$$

conditions that the eigenvectors and eigenvalues of H have to meet, in order for the system to provide perfect transfer at some $t \leq T$. This enables us to compare the number of free parameters in our setting with the number of conditions.

An ensemble of k sites has the site *in* and *out* fixed, leaving $k - 2$ intermediate atoms to move. They have d coordinates in d dimensions, which results in $d \cdot (k - 2)$ independent choices for the spatial setup. We do not fix the point in time at which a configuration has to transfer the excitation with unit efficiency, so time is an additional degree of freedom we have to consider. The number of free parameters is therefore $f = d \cdot (k - 2) + 1$ and the difference of interest, $s = f - c$ becomes

$$s = f - c = d \cdot (k - 2) + 1 - 2k + 3 = (d - 2) \cdot (k - 2). \tag{4.11}$$

First of all, this formula results in negative values of s for all $k \geq 3$ if $d = 1$, meaning configurations that exhibit perfect transfer do not exist in one dimension. However, we found examples of configurations that reach efficiencies as high as 99.897% for $k = 4$ and $T = 0.5 \cdot T_{Rabi}$. In fact, increasing the number of atoms further approaches the maximal efficiencies one can find to 1, but, as expected, no configurations have been found that yield perfect transfer $\mathcal{P} = 1$.

In the case of higher dimensions, we obtain $s = 0$ for $d = 2$ and $s = k - 2$ for $d = 3$. The number s can be interpreted as the dimension of a manifold in the space of all possible configurations at all possible times, on which the configurations providing optimal state transfer have to lie. For $s = 0$, the set of configurations is therefore discrete, though it does not have to be finite. This is consistent with the findings in chapter 3. In three dimensions, however, the manifold will be of dimension $s \geq 1$ for one or more intermediate sites, meaning there exist possibilities to change the configuration of the intermediate atoms by an infinitesimal amount without lowering the efficiency (although optimal transfer might then be obtained at a different point in time).

4.3 Generalized Centrosymmetry

In the previous section 4.1, we showed that centrosymmetry is sufficient to guarantee equal overlaps for eigenvectors with *in* and *out*. It is obvious that configurations which are spatially symmetric in the sense discussed in chapter 3 lead to a Hamiltonian that commutes with J, therefore their appearance in our calculations is not surprising. In contrast, we also found configurations that are not centrosymmetric and still fulfilled the necessary conditions.

This is why we will present a more general form of the Hamiltonian. We then show that Hamiltonians of this form are guaranteed to meet the condition of equal overlaps (4.6).

To find this form, let us diagonalize the $(k-2) \times (k-2)$ submatrix H_C in the center of H:

$$\mathcal{E} = U_C^\dagger \, H_C \, U_C = \mathrm{diag}(\varepsilon_2, \dots, \varepsilon_{k-1}), \tag{4.12}$$

where U_C is the matrix containing the eigenvectors H_C in its columns.

Next, we form the tensor product

$$U = \mathbb{1} \otimes U_C \otimes \mathbb{1} = \begin{bmatrix} 1 & 0 & \dots & \dots & 0 \\ 0 & & & & \vdots \\ \vdots & & U_C & & \vdots \\ \vdots & & & & 0 \\ 0 & \dots & \dots & 0 & 1 \end{bmatrix}, \tag{4.13}$$

which we can use to calculate the transform of the entire Hamiltonian via

$$H_T = U^\dagger \, H \, U. \tag{4.14}$$

Finally, we will show that if the result of this transformation is of the form

$$H_T = \begin{bmatrix} 0 & a_2 & a_3 & \dots & a_{k-1} & \frac{1}{8} \\ a_2 & \varepsilon_2 & & & & \pm a_2 \\ a_3 & & \varepsilon_3 & & & \pm a_3 \\ \vdots & & & \ddots & & \vdots \\ a_{k-1} & & & & \varepsilon_{k-1} & \pm a_{k-1} \\ \frac{1}{8} & \pm a_2 & \pm a_3 & \dots & \pm a_{k-1} & 0 \end{bmatrix} \tag{4.15}$$

then each eigenvector of this Hamiltonian has equal overlap with $|in\rangle$ and $|out\rangle$. The $\pm$ signs have to be understood as independent from each other for each index.

We explicitly write the time-independent Schrödinger equation:

$$H_T \, |v_i\rangle = \begin{bmatrix} 0 & a_2 & a_3 & \dots & a_{k-1} & \frac{1}{8} \\ a_2 & \varepsilon_2 & & & & \pm a_2 \\ a_3 & & \varepsilon_3 & & & \pm a_3 \\ \vdots & & & \ddots & & \vdots \\ a_{k-1} & & & & \varepsilon_{k-1} & \pm a_{k-1} \\ \frac{1}{8} & \pm a_2 & \pm a_3 & \dots & \pm a_{k-1} & 0 \end{bmatrix} \begin{bmatrix} v_{i,1} \\ v_{i,2} \\ \vdots \\ \vdots \\ v_{i,k-1} \\ v_{i,k} \end{bmatrix} = E_i \begin{bmatrix} v_{i,1} \\ v_{i,2} \\ \vdots \\ \vdots \\ v_{i,k-1} \\ v_{i,k} \end{bmatrix} \quad \forall i. \tag{4.16}$$

Note that the direct comparison of the first and last entry in the eigenvectors as overlap with $|in\rangle$ and $|out\rangle$ in the new basis is only possible because U leaves the positions of *in* and *out* unchanged, so the overlaps of the Hamiltonian in this basis are the same as the ones in the basis of site excitations $\{|i\rangle\}$. Because of the particular form for H we requested, 3 different kinds of equations can be extracted from Eq.(4.16) for a fixed i (which will be omitted for reasons of readability):

$$\frac{1}{8}\,v_k + \sum_{j=2}^{k-1} a_j\,v_j \;=\; E\,v_1, \tag{4.17}$$

$$a_j\,(v_1 \pm v_k) + \varepsilon_j\,v_j \;=\; E\,v_j, \quad j = \{2, 3, ..., k-1\}, \tag{4.18}$$

$$\frac{1}{8}\,v_1 + \sum_{j=2}^{k-1} \pm a_j\,v_j \;=\; E\,v_k. \tag{4.19}$$

We can also write Eq.(4.18) as

$$v_j = \frac{a_j(v_1 \pm v_k)}{E - \varepsilon_j}, \quad j = \{2, 3, ..., k-1\}, \tag{4.18*}$$

and insert this expression in Eq.(4.17) and (4.19):

$$\frac{1}{8}v_k + \sum_{j=2}^{k-1} a_j^2\,\frac{(v_1 \pm v_k)}{E - \varepsilon_j} = E\,v_1, \tag{4.17*}$$

$$\frac{1}{8}v_1 + \sum_{j=2}^{k-1} \pm a_j^2\,\frac{(v_1 \pm v_k)}{E - \varepsilon_j} = E\,v_k. \tag{4.19*}$$

By separating the sums and ordering the equations for v_k and v_1 we obtain two very similar equations (we set $a_j^2\,\dfrac{v_1 \pm v_k}{E - \varepsilon_j} =: b_j$ for simplicity):

$$v_1 = \frac{\frac{1}{8} + \sum_{j=2}^{k-1} \pm b_j}{E - \sum_{j=2}^{k-1} b_j}\,v_k =: A\,v_k, \tag{4.17**}$$

$$v_1 = \frac{E - \sum_{j=2}^{k-1} b_j}{\frac{1}{8} + \sum_{j=2}^{k-1} \pm b_j}\,v_k = A^{-1}\,v_k, \tag{4.19**}$$

$$\Rightarrow v_k = A^2\,v_k. \tag{4.20}$$

The fraction A has to be of modulus 1, so we conclude

$$v_1 = \pm v_k, \tag{4.21}$$

which is what we wanted to show.

In order to guarantee that H_T is of the required form, we only need to fulfill $(k-2)$ conditions, namely pairwise equal modulus for the entries in the first row and the last column, respectively. This agrees with our arguments in section 4.2, according to which equal overlap of all eigenvectors with *in* and *out* can be reached with $(k-2)$ conditions.

Chapter 5

Hessian Matrix Analysis

In this chapter, we want to confirm our conclusions of chapter 4.2 (concerning the dimension of the set of configurations giving rise to perfect transfer) by investigating the infinitesimal neighborhood of a perfect configuration.

For this purpose, we look at the configurations as vectors in a $d \cdot (k - 2) + 1$ dimensional vector space, that contain the positions of all intermediate atoms and the time coordinate t (remember that the positions of *in* and *out* are fixed, so we can reduce the problem to the subspace where their coordinates do not appear):

$$\vec{x} = (\vec{r}_2, \ldots, \vec{r}_{k-1}, t). \tag{5.1}$$

From the results of chapter 4, we expect that the set of optimal configurations is a manifold (with dimension $s = 0$ for $d = 2$ and $s = k - 2$ for $d = 3$) contained inside this space. If we assume that $\vec{x}_0$ is an optimal configuration, then a Taylor series expansion of $\mathcal{P}(\vec{x})$ around such a maximum can be written as

$$\mathcal{P}(\vec{x}) = 1 + \underbrace{\boldsymbol{\nabla}\mathcal{P}^\top}_{\approx 0} (\vec{x} - \vec{x}_0) + \frac{1}{2}(\vec{x} - \vec{x}_0)^\top M_H (\vec{x} - \vec{x}_0) + \mathcal{O}((\vec{x} - \vec{x}_0)^3), \tag{5.2}$$

$$\Rightarrow \Delta\mathcal{P}(\vec{x}) = \mathcal{P}(\vec{x}) - \mathcal{P}(\vec{x}_0) \approx \frac{1}{2}(\vec{x} - \vec{x}_0)^\top M_H (\vec{x} - \vec{x}_0), \tag{5.3}$$

where $\vec{x}_0$ is optimal the configuration, $\vec{x}$ a configuration nearby and M_H the Hessian matrix containing the second partial derivatives evaluated at $\vec{x}_0$. The derivatives are calculated approximatively with the difference quotient. As a notation, we use

$$\mathcal{P}_{(x_i\pm, x_j\pm)} := \mathcal{P}(x_1, \ldots, x_i \pm \Delta x, \ldots, x_j \pm \Delta x, \ldots, t), \tag{5.4}$$

where the x_i runs over all spatial coordinates and time. For $i \neq j$ the difference quotient is

$$\frac{\partial^2 \mathcal{P}}{\partial x_i \partial x_j} \approx \frac{\mathcal{P}_{(x_i+, x_j+)} + \mathcal{P}_{(x_i-, x_j-)} - \mathcal{P}_{(x_i-, x_j+)} - \mathcal{P}_{(x_i+, x_j-)}}{4 (\Delta x)^2}, \tag{5.5}$$

whereas for $i = j$, we calculate

$$\frac{\partial^2 \mathcal{P}}{(\partial x_i)^2} \approx \frac{\mathcal{P}(x_1, \ldots, x_i + \Delta x, \ldots, t) + \mathcal{P}(x_1, \ldots, x_i - \Delta x, \ldots, t) - 2\,\mathcal{P}(\vec{x}_0)}{(\Delta x)^2}. \tag{5.6}$$

The change in transfer probability should always be negative for the two-dimensional case (only isolated maxima should appear), so the matrix is expected to be negative definite which is easily verified by calculating the eigenvalues and checking whether all of them are negative and distinctly nonzero. In three dimensions, however, apart from only negative eigenvalues, we expect $(k-2)$ of them to be zero, such that we can move the configuration along the $(k-2)$-dimensional manifold without decreasing the transfer efficiency.

5.1 2D Configurations

From a numerical point of view, we have to be careful when choosing the stepsize $\triangle x$. If it is too large, the approximation is not sufficiently accurate, but if it is very small, computational errors add up and distort the actual values of the function of interest. To analyze this, we inspected the dependence of the smallest eigenvalue on the stepsize for several configurations and obtained a plot where a plateau is visible. We judge the center of this plateau to be a good choice, since the eigenvalue is stable in this region. An example, which belongs to configuration no. 2 in Table 5.1 is shown in Fig. 5.1.
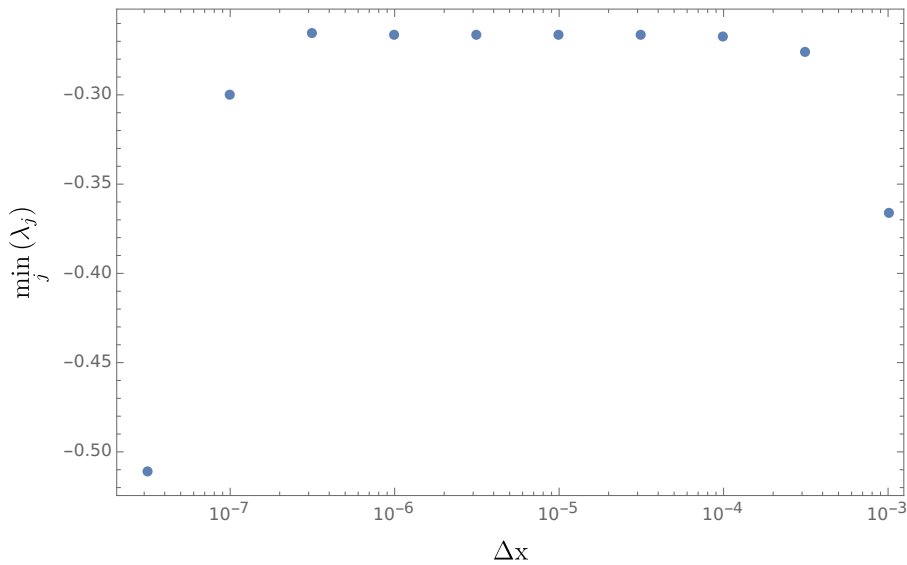
Figure 5.1: The dependence of the smallest eigenvalue of example configuration no. 2 in Table 5.1 on the chosen stepsize $\triangle x$ in numerical differentiation. We chose $\triangle x = 5 \times 10^{-5}$ for the 2D calculations.

Tables 5.1 to 5.5 show the largest and the four smallest eigenvalues for two-dimensional configurations of 4 to 8 atoms with four randomly chosen examples of optimal configurations each. The values cover almost in all cases between 4 and 5 orders of magnitude, which is indicating a complicated potential surface of the function $\mathcal{P}$, even near the maxima. As we expected, the eigenvalues are always strictly smaller than zero.

Example No.	Largest EV	4 Smallest Eigenvalues			
1	-5737.14	-157.301	-32.170	-1.391	-0.167
2	-4652.23	-567.858	-21.026	-0.434	-0.267
3	-5501.19	-805.894	-24.957	-3.832	-0.067
4	-1052.41	-118.326	-28.332	-3.563	-0.852

Table 5.1: Examples of eigenvalues for a Hessian belonging to perfect configurations of 4 atoms in 2D

Example No.	Largest EV	4 Smallest Eigenvalues			
1	-3251.25	-13.123	-4.497	-1.289	-0.043
2	-1272.10	-20.716	-8.745	-3.181	-0.332
3	-1507.30	-131.32	-3.591	-1.762	-0.048
4	-2623.32	-8.914	-6.620	-0.933	-0.562

Table 5.2: Examples of eigenvalues for a Hessian belonging to perfect configurations of 5 atoms in 2D

In table 5.2 to 5.5 one can see that in general, all eigenvalues remain strictly smaller than zero, but the magnitude of the smallest one is decreasing with growing number of atoms k. This is compatible with the observation of a larger number of perfect configurations for higher k in chapter 3, as a smaller decrease in probability near a maximum makes it possible for other maxima to lie closer.

Example No.	Largest EV	4 Smallest Eigenvalues			
1	-419.543	-0.2546	-0.1328	-0.0225	-0.0061
2	-345.607	-2.4117	-0.8169	-0.1799	-0.0455
3	-652.031	-0.9770	-0.1656	-0.0109	-0.0010
4	-1079.09	-1.1598	-0.2381	-0.0703	-0.0174

Table 5.3: Examples of eigenvalues for a Hessian belonging to perfect configurations of 6 atoms in 2D

Example No.	Largest EV	4 Smallest Eigenvalues			
1	-485.244	-1.6070	-0.9128	-0.0665	-0.0130
2	-275.907	-1.8624	-0.9849	-0.6988	-0.0039
3	-584.077	-0.5286	-0.3694	-0.0923	-0.0065
4	-614.527	-1.44876	-0.0945	-0.0179	-0.0083

Table 5.4: Examples of eigenvalues for a Hessian belonging to perfect configurations of 7 atoms in 2D

Example No.	Largest EV	4 Smallest Eigenvalues			
1	-351.396	-1.2627	-0.3528	-0.2258	-0.00681
2	-1798.71	-0.5381	-0.0532	-0.0144	-0.00013
3	-916.419	-0.5931	-0.2558	-0.0307	-0.00570
4	-439.275	-0.7705	-0.3247	-0.0505	-0.01316

Table 5.5: Examples of eigenvalues for a Hessian belonging to perfect configurations of 8 atoms in 2D

5.2 3D Configurations

Following the considerations for two dimensions, we move on to analyzing some 3D examples in detail, again for a number of atoms ranging from 4 to 8. In the corresponding tables 5.6 to 5.10, we have omitted the largest eigenvalue, since it behaves in a similar way as for two dimensions. To check whether there actually are $k-2$ eigenvalues equal to zero, we look at the smallest k ones. For $k=4$ we expect $4-2=2$ eigenvalues to be zero. In Table 5.6 one can indeed identify two values that are at least three orders of magnitude smaller than the others, but similar compared to each other (at most a factor of 10 difference). In the tables for higher k we also find the expected $k-2$ eigenvalues that are very close to zero and sometimes positive. The occurence of positive values (marked in bold font) is actually a sign that we reached zero in the range of our precision. To visualize this, we also plotted the dependence of the smallest eigenvalue of configuration no. 1 in Table 5.6 on the chosen stepsize in Fig. 5.2. One can see that the sign of this value actually changes its sign depending on Δx, meaning that the error made due to our choice of finite stepsize is in the range of 10^{-5}.

Ex. No.	4 Smallest Eigenvalues			
1	-3.581	-0.210	$-2.2 \cdot 10^{-5}$	$-1.2 \cdot 10^{-5}$
2	-1.392	-0.178	$-2.5 \cdot 10^{-4}$	$-1.4 \cdot 10^{-4}$
3	-3.208	-1.983	$-3.4 \cdot 10^{-5}$	$-1.6 \cdot 10^{-5}$
4	-3.137	-2.111	$-3.2 \cdot 10^{-5}$	$-1.9 \cdot 10^{-5}$

Table 5.6: Examples of eigenvalues for a Hessian belonging to perfect configurations of 4 atoms in 3D

Ex. No.	5 Smallest Eigenvalues				
1	-1.903	-1.060	$-3.1 \cdot 10^{-5}$	$-1.4 \cdot 10^{-5}$	$-1.2 \cdot 10^{-6}$
2	-1.162	-0.463	$-2.5 \cdot 10^{-4}$	$-7.4 \cdot 10^{-5}$	$-1.6 \cdot 10^{-5}$
3	-1.622	-2.047	$-3.0 \cdot 10^{-5}$	$-1.95 \cdot 10^{-5}$	$-7.9 \cdot 10^{-6}$
4	-0.041	-0.026	$-1.4 \cdot 10^{-4}$	$-2.0 \cdot 10^{-5}$	$-1.3 \cdot 10^{-5}$

Table 5.7: Examples of eigenvalues for a Hessian belonging to perfect configurations of 5 atoms in 3D

Ex. No.	6 Smallest Eigenvalues					
1	-0.149	-0.102	$-4.05 \cdot 10^{-5}$	$-2.9 \cdot 10^{-5}$	$-2.0 \cdot 10^{-5}$	$-1.5 \cdot 10^{-5}$
2	-1.142	-0.556	$-3.1 \cdot 10^{-5}$	$-2.1 \cdot 10^{-5}$	$-1.3 \cdot 10^{-5}$	$-1.2 \cdot 10^{-5}$
3	-0.920	-0.577	$-1.7 \cdot 10^{-5}$	$\mathbf{5.4 \cdot 10^{-6}}$	$-4.7 \cdot 10^{-6}$	$\mathbf{8.8 \cdot 10^{-7}}$
4	-0.876	-0.692	$\mathbf{1.9 \cdot 10^{-5}}$	$\mathbf{1.0 \cdot 10^{-5}}$	$-9.8 \cdot 10^{-6}$	$-3.0 \cdot 10^{-6}$

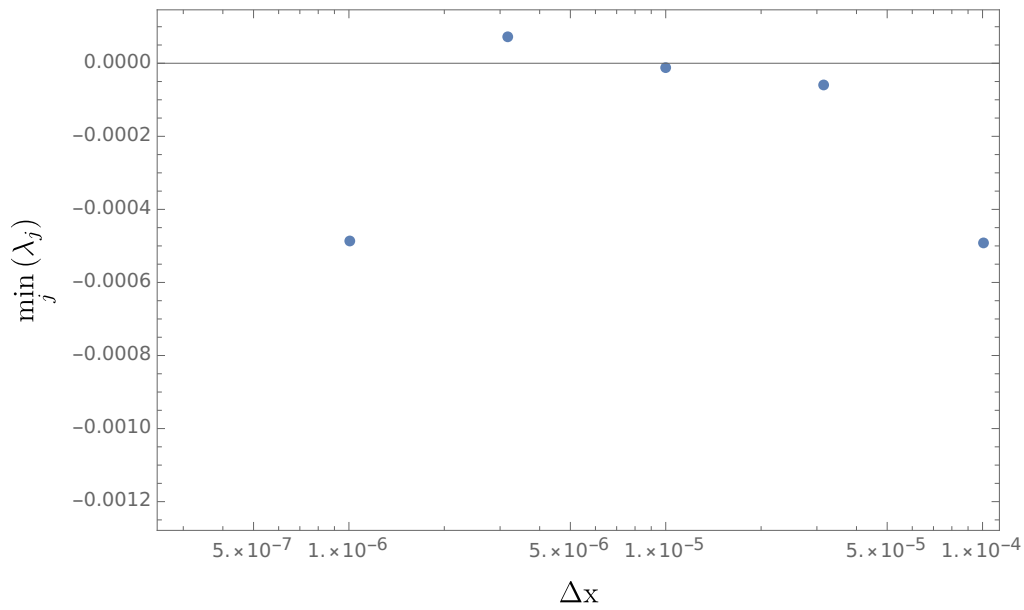Table 5.8: Examples of eigenvalues for a Hessian belonging to perfect configurations of 6 atoms in 3D

Figure 5.2: The dependence of the smallest eigenvalue of example configuration no. 1 in Table 5.6 on the chosen stepsize Δx in numerical differentiation. We chose $\Delta x = 10^{-5}$ for the 3D calculations.

Ex. No.	7 Smallest Eigenvalues						
1	-0.160	-0.099	$-4.8 \cdot 10^{-5}$	$-4.0 \cdot 10^{-5}$	$-3.1 \cdot 10^{-5}$	$-2.3 \cdot 10^{-5}$	$-2.0 \cdot 10^{-5}$
2	-0.198	-0.082	$-4.7 \cdot 10^{-5}$	$-4.0 \cdot 10^{-5}$	$-3.2 \cdot 10^{-5}$	$-2.2 \cdot 10^{-5}$	$-1.0 \cdot 10^{-5}$
3	-0.180	-0.033	$-2.7 \cdot 10^{-5}$	$-1.7 \cdot 10^{-5}$	$\mathbf{8.7 \cdot 10^{-6}}$	$-7.0 \cdot 10^{-6}$	$-3.3 \cdot 10^{-6}$
4	-0.040	-0.005	$\mathbf{3.5 \cdot 10^{-5}}$	$\mathbf{2.1 \cdot 10^{-5}}$	$\mathbf{1.6 \cdot 10^{-5}}$	$-1.0 \cdot 10^{-5}$	$-9.1 \cdot 10^{-6}$

Table 5.9: Examples of eigenvalues for a Hessian belonging to perfect configurations of 7 atoms in 3D

Ex. No.	8 Smallest Eigenvalues							
1	-0.60	-0.32	$-5.3 \cdot 10^{-5}$	$-4.5 \cdot 10^{-5}$	$-3.5 \cdot 10^{-5}$	$-3.1 \cdot 10^{-5}$	$-3.0 \cdot 10^{-5}$	$-1.8 \cdot 10^{-5}$
2	-0.30	-0.01	$-4.6 \cdot 10^{-5}$	$-2.4 \cdot 10^{-5}$	$-2.2 \cdot 10^{-5}$	$-1.2 \cdot 10^{-5}$	$\mathbf{1.1 \cdot 10^{-5}}$	$-6.1 \cdot 10^{-6}$
3	-0.09	-0.01	$-5.7 \cdot 10^{-5}$	$-4.5 \cdot 10^{-5}$	$-3.6 \cdot 10^{-5}$	$-3.1 \cdot 10^{-5}$	$-3.0 \cdot 10^{-5}$	$-1.6 \cdot 10^{-5}$
4	-0.38	-0.01	$-1.5 \cdot 10^{-5}$	$\mathbf{1.5 \cdot 10^{-5}}$	$\mathbf{1.3 \cdot 10^{-5}}$	$\mathbf{9.6 \cdot 10^{-6}}$	$\mathbf{6.5 \cdot 10^{-6}}$	$-2.4 \cdot 10^{-6}$

Table 5.10: Examples of eigenvalues for a Hessian belonging to perfect configurations of 8 atoms in 3D

To numerical accuracy, the existence of $k - 2$ eigenvalues equal to zero has been confirmed. Together with the results of section 5.1, we have therefore verified our predictions. As a different method of verification, perturbation theory up to second order would provide a means to calculate M_H exactly (i.e. without relying on finite differences).

Conclusion and Outlook

We investigated transfer of single excitations mediated by dipole-dipole interaction in unordered networks of Rydberg-atoms. We focused on finding and characterizing configurations of atoms that were able to transfer the excitation from one end of the network to the other with perfect efficiency. Motivated by the experimental constraints of discrete distances between Rydberg atoms in a two-dimensional optical array, we checked all possible configurations for a chosen lattice geometry that were attainable in a reasonable amount of time. The best candidates we found in this approach reached over 99% transfer efficiency in under 1/5 of the Rabi oscillation period, which is surprising, given their simple setup. To gain further insight in the distribution of highly efficient configurations in two dimensions, we sampled continuously in the $\mathbb{R}^2$ unit disk and optimized the transport efficiencies to practically unity. For a number of sites from $k = 4$ to $k = 7$, we found discrete sets of configurations exhibiting increasingly smaller transfer times. In an attempt to understand this result analytically, we relied on earlier work in the field, where necessary and sufficient conditions for perfect state transfer had been derived. We compared the number of these conditions with the number of variable parameters in our problem. This allowed us to predict the dimension s for the manifold of perfect configurations one can find in the $d \cdot (k - 2) + 1$-dimensional space of configurations, where d is the dimension of the Euclidean space the Rydberg atoms are placed in. For $d = 2$, we obtained $s = 0$, which is consistent with the observed discrete set of solutions. The prediction for $d = 3$ was $s = k - 2$. Finally, we were able to confirm these considerations by evaluating the behaviour of the transfer efficiency in an infinitesimal neighborhood around several optimal configurations: The Hessian matrix of a Taylor approximation up to second order contained the expected $k - 2$ eigenvalues equal to zero in the three dimensional case, while all eigenvalues were distinctly negative in two dimensions.

In our opinion, our findings give rise to at least three open questions left for future work. First of all, it would be interesting to further characterize the manifolds of perfect configurations in three dimensions. Secondly, we found signs that symmetric configurations in general provide faster transport than asymmetric ones for an equal number of sites involved, but we did not have enough time to perform the necessary analysis. The last open point comes from an especially surprising result, which we were not able to understand so far: In two dimensions, a large number of configurations reach transport efficiencies $\mathcal{P} \geq 1 - 10^{-6}$, which is already very close to unity, but most of them did not appear in our sets with $\mathcal{P} \geq 1 - 10^{-13}$. We are convinced that the answers to the presented problems could contribute to understanding our findings even better.

Appendix

A: Ensembles of optimized configurations with $\mathcal{P} \geq 1 \text{-} 10^{-6}$

Comparing these ensembles with the ones for quasi-perfect transfer ($\mathcal{P} \geq 1 - 10^{-13}$), see Fig. 3.1, 3.3, 3.5 and 3.6, we see a much larger number of configurations. In other words, the function $\mathcal{P}(\vec{x})$ exhibits many local maxima with $1 - 10^{-6} \leq \mathcal{P} \leq 1 - 10^{-13}$.
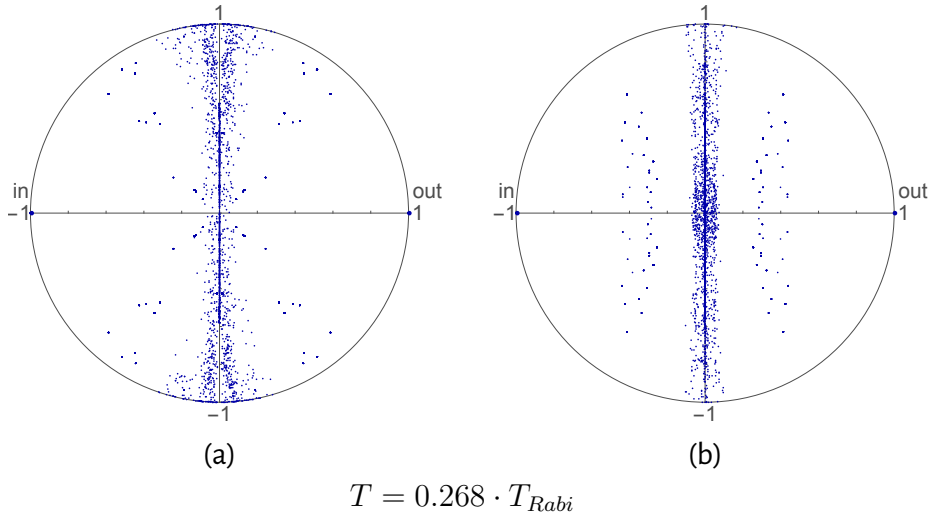

$$T = 0.268 \cdot T_{Rabi}$$

Figure 5.3: Asymmetric (a) and symmetric (b) configurations with 5 atoms

$$T = 0.113 \cdot T_{Rabi}$$
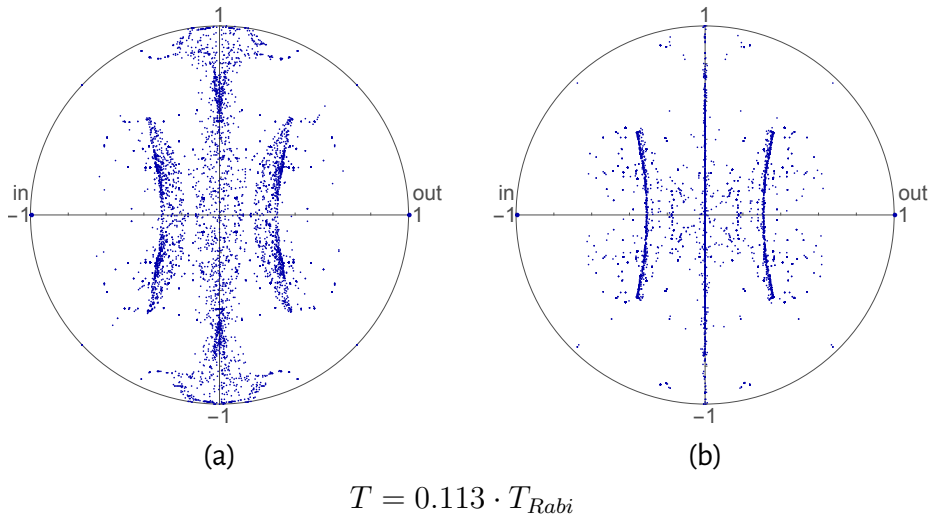
Figure 5.4: Asymmetric (a) and symmetric (b) configurations with 6 atoms
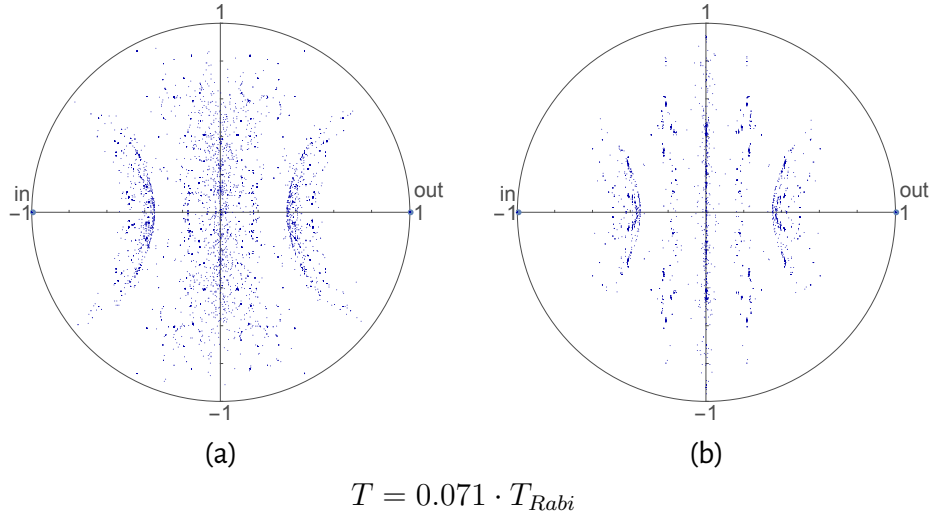
$$T = 0.071 \cdot T_{Rabi}$$

Figure 5.5: Asymmetric (a) and symmetric (b) configurations with 7 atoms

B: Transfer Times of the Best Configurations on Lattices

N×N	4	5	6	7	8
5	0.093	0.090	0.033	0.100	0.097
7	0.065	0.064	0.089	0.082	0.095
9	0.096	0.095	0.089		
11	0.090	0.094	0.092		
13	0.070	0.090			

Table 5.11: Transfer times for efficiencies in 2.1

N×N	4	5	6	7	8
5x5	0.200	0.200	0.194	0.200	0.097
7x7	0.065	0.189	0.188	0.191	0.196
9x9	0.200	0.200	0.188		
11x11	0.128	0.196	0.185		
13x13	0.070	0.189			

Table 5.12: Transfer times for efficiencies in 2.2

C: Coordinates of the Fastest Continuous Configurations with $\mathcal{P} \geq 1 - 10^{-13}$

The input and output atom corresponding to number 1 and k are always located at positions S_1(-1,0) and S_k(1,0).

k=4		
Atom no.	x	y
2	-0.109945	0.400635
3	0.109945	-0.400635

Coordinates of configuration 3.2

k=5 / asymmetric		
Atom no.	x	y
2	0.087902	-0.072491
3	0.448099	-0.739210
4	-0.342488	-0.527398

Coordinates of configuration 3.7(a)

k=5 / symmetric		
Atom no.	x	y
2	0	0.030097
3	0.424101	0.481339
4	-0.424101	0.481339

Coordinates of configuration 3.7(b)

k=6 / asymmetric		
Atom no.	x	y
2	-0.549726	-0.286648
3	-0.160786	-0.239383
4	0.214369	-0.388046
5	0.607648	-0.362172

Coordinates of configuration 3.8(a)

k=6 / symmetric		
Atom no.	x	y
2	0.461219	-0.259108
3	-0.461219	0.259108
4	0.166140	0.082400
5	-0.166140	-0.082400

Coordinates of configuration 3.8(b)

k=7 / asymmetric		
Atom no.	x	y
2	-0.534041	-0.255531
3	0.093079	0.142185
4	-0.165364	-0.216863
5	0.474138	-0.075842
6	0.081314	-0.170088

Coordinates of configuration Fasion 3.9(a)

k=7 / symmetric		
Atom no.	x	y
2	0.161490	-0.168353
3	0.494887	0.024776
4	0	0.245163
5	-0.494887	0.024775
6	-0.161489	-0.168353

Coordinates of configuration 3.9(b)

Bibliography

[1] R.E. Fenna and B.W. Matthews. Chlorophyll arrangement in a bacteriochlorophyll protein from chlorobium limicola. *Nature*, 258:573–577, 1975.
`http://dx.doi.org/10.1038/258573a0`.

[2] J. Dostál, J. Pšenčík, and D. Zigmantas. *In situ* mapping of the energy flow through the entire photosynthetic apparatus. *Nature Chemistry*, 8:705–710, 2016. `http://dx.doi.org/10.1038/nchem.2525`.

[3] J. Adolphs and T. Renger. How proteins trigger excitation energy transfer in the fmo complex of green sulfur bacteria. *Biophysical Journal*, 91:2778–2797, 2006. `http://dx.doi.org/10.1529/biophysj.105.079483`.

[4] V. Kostak, G. M. Nikolopoulos, and I. Jex. Perfect state transfer in networks of arbitrary topology and coupling configuration. *Physical Review A*, 75:042319, 2007.
`http://dx.doi.org/10.1103/PhysRevA.75.042319`.

[5] T. R. Engel, G. S., T. R. Calhoun, E. L. Read, T.-K. Ahn, T. Mancal, Y.-C. Cheng, R. E. Blankenship, and G. Fleming. Evidence for wavelike energy transfer through quantum coherence in photosynthetic systems. *Nature*, 446:782–786, 2007.
`http://dx.doi.org/10.1038/nature05678`.

[6] G. Günter, H. Schempp, M. Robert-de Saint-Vincent, V. Gavryusev, S. Helmrich, C.S. Hofmann, S. Whitlock, and M. Weidemüller. Observing the dynamics of dipole-mediated energy transport by interaction-enhanced imaging. *Science*, 342:954–956, 2013. `http://dx.doi.org/10.1126/science.1244843`.

[7] M. Schlosser, S. Tichelmann, J. Kruse, and G. Birkl. Scalable architecture for quantum information processing with atoms in optical micro-structures. *Quantum Information Processing*, 10(6):907, 2011.
`http://dx.doi.org/10.1007/s11128-011-0297-z`.

[8] T. Scholak, T. Wellens, and A. Buchleitner. Spectral backbone of excitation transport in ultracold rydberg gases. *Physical Review A*, 90:063415, 2014.
`http://dx.doi.org/10.1103/PhysRevA.90.063415`.

[9] Torsten Scholak. *Transport and coherence in disordered networks*. PhD thesis, Universitätsbibliothek Freiburg, 2011.
`http://www.freidok.uni-freiburg.de/volltexte/8283/`.

[10] Torsten Scholak, Fernando de Melo, Thomas Wellens, Florian Mintert, and Andreas Buchleitner. Efficient and coherent excitation transfer across disordered molecular networks. *Phys. Rev. E*, 83:021912, 2011.
https://dx.doi.org/10.1103/PhysRevE.83.021912.

[11] Torsten Scholak, Thomas Wellens, and Andreas Buchleitner. Optimal networks for excitonic energy transport. *Journal of Physics B: Atomic, Molecular and Optical Physics*, 44(18): 184012, 2011.
http://stacks.iop.org/0953-4075/44/i=18/a=184012.

[12] W.H. Press, S.A. Teukolsky, W.T. Vetterling, and B.P. Flannery. *Numerical Recipes in C*. Cambridge University Press, 2nd edition, 2002.

[13] M. Walschaers, J Fernandez-de Cossio Diaz, R. Mulet, and A. Buchleitner. Optimally designed quantum transport across disordered networks. *Physical Review Letters*, 111:180601, 2013.
http://dx.doi.org/10.1103/PhysRevLett.111.180601.

[14] M. Walschaers, R. Mulet, T. Wellens, and A. Buchleitner. Statistical theory of designed quantum transport across disordered networks. *Physical Review E*, 91:042137, 2015.
http://dx.doi.org/10.1103/PhysRevE.91.042137.

Eidesstattliche Erklärung

Hiermit versichere ich, die vorliegende Bachelorarbeit

„Optimal Excitation Transfer in two-dimensional Lattices of Rydberg-atoms"

eigenständig verfasst und ausschließlich die angegebenen Quellen und Hilfsmittel benutzt zu haben. Wörtlich oder inhaltlich verwendete Quellen wurden entsprechend den anerkannten Regeln wissenschaftlichen Arbeitens zitiert. Ich erkläre desweiteren, dass die vorliegende Arbeit noch nicht in gleicher oder ähnlicher Ausführung Bestandteil einer Prüfungsleistung war.

Freiburg, den 3. August 2017

_____

Dominik Bäuerle